

Turbulent Channel Flow  
under the action of surface wind-stress

Yu Xu Qing

2 - 87

The Administration of North-West  
Electric Power System  
Xian, China

Report nr. 2 - 87  
Technical University Delft  
Faculty of Civil Engineering  
Laboratory of Fluid Mechanics

## Abstract

This report deals with experimental research into the wind profile and turbulent current distribution measurements in a wind-water tunnel. Most attention was paid to the water velocity profile as influenced by the wind. It is confirmed that the velocity distribution of the current essentially follows the log law near the air-water interface as well as near the bottom of the channel. In the case of opposing wind action, the current profile is separated from the point of stress reversal into two regions, the upper and lower region, and it can be approximated by fitting two logarithmic curves. In the case of both opposing and following action, Reid's (ref. 6) generalized formula for the current profile was used to analyse the experimental results and the estimated responses agree well with the data. In addition, the general character of  $m$  (ratio of bottom stress to surface stress) was also discussed graphically in Fig. 25.

## I Introduction

Early work, intensive studies and measurements of wind-wave interactions have primarily concentrated on phenomena at the air-water interface see Keulegan 1951; Baines & Knapp 1965; Plate 1970; Shemdin 1972 etc.

A study on the turbulent structure of currents under the action of wind shear has recently been made by Hiroichi Tsuruya (ref. 2). In this study the mean wind and water velocity has an opposite sign. It was shown that the friction velocity of the water flow at the free surface  $U_{*w}$  remains uncertain. Moreover, without taking into account the different current flows, the adoption of  $m = -0.8$  as a constant, which is the ratio of shear stress at the bed to the water surface for a certain wind action is still questionable.

The purpose of this research is to reexamine the characteristics of the water turbulent motion under the action of wind shear.

## II Experiment

The main part of the experimental installation was a wind flume with 80 cm by 59 cm cross section, nearly 38 m long.

The flume had a plywood roof, glass side walls and a plastered bottom (Fig. 1). At the ends of the flume a suction ventilator and air intake were presented. The position of this two devices, the ventilator and intake could be reversed when necessary to change the direction of air flow. Close to the ventilator a part of the plywood roof of the flume was movable, and hence the opening width of this section could be adjusted to obtain different air velocities through the tunnel. In the present experiment, the air velocities at 10 cm above the water surface varied from 3.7 m/s to 8 m/s.

The water currents were generated by a water supply pipeline system at one end wall of the flume and sluice gates at the other end. In this way the flow rate and the water depth could be controlled.

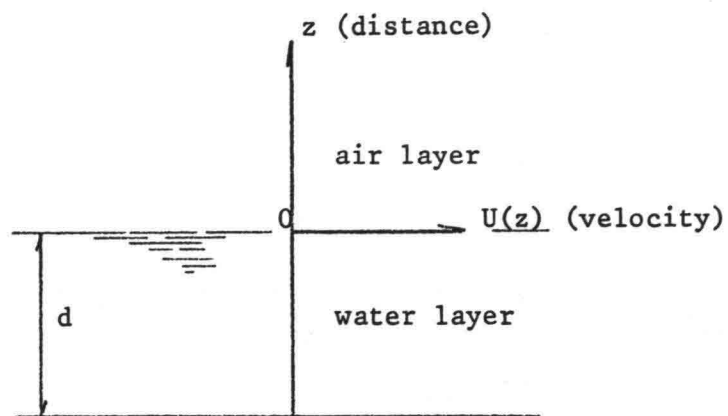
The flow rate was measured by means of Venturimeter and manometer.

In preliminary test, wind waves were found to develop where the wind velocity was higher than 3.5 m/s. To suppress them for the greater, a surfactant (teepol, SHELL detergent) was applied to the upper layer. It was confirmed that adding the surfactant did not noticeably alter the surface shear stress (ref. 2, 5).

The test section was located around the middle of the flume where the mean water surface is little affected by the wind-induced set up of the water surface. The water depth at the test section was kept constant at 20 cm. Observations were made of various water flow cases (see Table 2, 3) for three air-flow condition with mean velocities of 3.7; 5.7; 8.0 m/s, measured at 10 cm above the water surface. In each case, the mean velocity distribution were measured with a Pitot-static tube for the air flow and a Laser-Doppler velocity meter for the water flow. In addition, the surface velocity of the water was estimated by placing a small 5 mm diameter buoyant paper (saturated with parafin) on the water

and measuring the time required for it to move past two stations 50 cm upwind and down wind from the test section, respectively.

In the following analyses the coordinate system shown as below will be used.



### III Air layer

The measured wind velocity profiles near the air-water interface are well approximated by logarithmic curves. When taking the moving surface boundary into account, it may be represented by

$$U_s - U_a(Z) = \frac{U_{*a}}{K} \ln \frac{Z}{Z_{oa}} \quad (1)$$

in which,

$U_a(Z)$  = wind velocity at an elevation  $Z$  above the mean water surface.

$U_{*a}$  = friction velocity of the wind at the interface.

$Z$  = elevation measured from mean water surface.

$K$  = Von Karman constant taken to be 0.4.

$Z_{oa}$  = roughness length.

$U_s$  = surface velocity of water.

The friction velocity  $U_{*a}$  is related to the shear stress  $\tau_a$  by the relation  $U_{*a} = \sqrt{\tau_a / \rho_a}$ , where  $\rho_a$  is the density of air.

The observed profiles in the lower part 10 cm above water surface in the air layer are shown in Fig. 2 to Fig. 6.

The friction velocities  $U_{*a}$  were determined by applying Eq. 1 to the measured data. In the case of the neglect of wave drag, equivalent friction velocities  $U_{*s}$  in connection with water can be estimated following the relation of  $\rho_w U_{*s}^2 = \rho_a U_{*a}^2$  where  $\rho_w$  is the density of the water. The results were shown in Fig. 22.

From Fig. 22, it can be concluded that due to the small value of the surface velocity of water in comparison with the air velocity, the surface velocity  $U_s$  in eq. 1 may be neglected.

However, in the case of a low air velocity, such as 3.7 m/s (measured at 10 cm above water surface), the friction velocity will possibly change following the larger current flow, which could not be neglected.

#### IV Water layer (opposing wind action)

Laser-Doppler velocimetry was used to determine the mean velocity profiles in the water layer with and without wind action. The profiles were taken in the measuring station which is near the middle of the flume where the flow had become uniform. The results are shown in Fig. 7 to Fig. 21 (dot sign for wind action, circle for current only).

Due to the wind action against the current flow, a decrease of velocity with depth in the upper layers is seen, giving rise to a maximum velocity at some sub-surface level. The result is that, for a given discharge, the velocity shear near the bed is larger than what it would be in the case of the absence of the wind. The comparison in detail will be mentioned later.

In the flow without wind action, the current profile is well approximated by the logarithmic and the 1/7th power laws.

These two laws can be expressed as

$$U(Z) = \frac{U_{*b}}{K} \ln \frac{Z + D}{Z_{ob}} \quad (2)$$

$$U(Z) = U_s \left( \frac{Z + D}{D} \right)^{1/7} \quad (3)$$

in which,

$U(Z)$  mean velocity at an elevation  $Z$ .

$U_{*b}$  friction velocity at the bottom.

$Z_{ob}$  roughness length at the bed.

$D$  depth of water.

$U_s$  surface velocity.

The friction velocity at the bottom was estimated by applying eq. 2 to the observed data. The parameters used in calculating the relations are summarized in Table 1.

Table 1. Parameters in calculating eq. (2).

$U_w$ cm/s	4.75	10.4	14.1	18.0	21.4
$U_{*b}$ cm/s	0.365	0.681	0.864	1.106	1.232
$Z_{ob}$ cm	$4.94 \times 10^{-2}$	$1.32 \times 10^{-2}$	$7.933 \times 10^{-3}$	$6.36 \times 10^{-3}$	$3.188 \times 10^{-3}$
$U_s$	5.92	12.6	17.1	22.7	27.7

The thickness of the viscous sublayer  $\delta_o$  is commonly approximated by  $\delta_o = 11.6 \nu_w / U_{*b}$ , (ref. 11), in which  $\nu_w$  is kinematic viscosity of water. In all cases the magnitude of  $\delta_o$  is much larger than the roughness length  $Z_{ob}$ , therefore it may be regarded as hydraulically smooth regime. (ref. 11).

The agreement between experimental data (Fig. 7-21 & 26-37, circle) and relation (3) are reasonably well for all cases. However, for the relation (2) (log law) the results tend to be smaller than the observed data in the upper layer of the flow (Fig. 7-21, thick solid curve). The curves calculated from relation 3 are shown in Fig. 26-37, noted as P.

In the flow with wind action, Reid (ref. 6) has given a general treatment of steady state channel flows using the generalized mixing-length hypothesis of Montgomery and the presumed relationship between stress and velocity shear due to Prandtl and Von Karman. Its theoretical derivation has also been outlined in the Hiroichi Tsuruya report (ref. 2). This may be summarized as follows (for  $m < 0$ )

$$\frac{U(Z)}{U_{*w}} = -U_m - \frac{1}{K'} [B_o \ln \frac{B_o - Y}{B_o + Y} + 2 B_1 \tan^{-1} \frac{Y}{B_1}] \quad z < z_m \quad (4)$$

$$\frac{U(Z)}{U_{*w}} = -U_m - \frac{1}{K'} [2 B_o \tan^{-1} \frac{Y}{B_o} + B_1 \ln \frac{B_1 - Y}{B_1 + Y}] \quad z > z_m \quad (5)$$

$$U_m = \frac{1}{K'} [B_o \ln \frac{B_o + \sqrt{|m|}}{B_o - \sqrt{|m|}} - 2 B_1 \tan^{-1} \frac{\sqrt{|m|}}{B_1}] \quad (6)$$

$$m = \tau_b / \tau_s$$

$$\zeta = \frac{D + Z}{D}$$

$$\zeta_m = \frac{|m|}{1 + |m|}$$

$$Y = \sqrt{(m + (1 - m)\zeta)l}$$

$$B_0 = \sqrt{(1 - m)Y_0 - m}$$

$$B_1 = \sqrt{1 + (1 - m)Y_1}$$

$$K' = K(1 + Y_0 + Y_1)$$

$$Y_0 = Z_{ob}/D$$

$$Y_1 = Z_{ow}/D$$

(7)

in which,

$U_m$  = current velocity at  $\zeta = \zeta_m$  (maximum relative velocity in the case of negative  $m$ )

$U_{*w}$  = friction velocity of the current at the free surface

$\tau_s$  = shear stress at the water surface

$\tau_b$  = shear stress at the bed

$Z_{ow}$  = roughness length for the free surface in water

When  $Y_0, Y_1 \ll 1$  and  $m < 0$ , the surface velocity  $U_s$  and mean current velocity  $U_w$  are estimated as

$$\frac{U_o}{U_{*w}} = \frac{1}{K} \left[ \ln \frac{4}{(1+|m|)y_1} + 2 \tan^{-1} \sqrt{|m|} - \sqrt{|m|} \left\{ \ln \frac{4|m|}{(1+|m|)y_o} + 2 \tan^{-1} \frac{1}{\sqrt{|m|}} \right\} \right] \quad (8)$$

$$\frac{U_w}{U_{*w}} = \frac{2}{K} \left[ 1 + \sqrt{|m|} - B_o \left( \tan^{-1} \frac{1}{B_o} + \frac{1}{2} \ln \frac{B_o + \sqrt{|m|}}{B_o - \sqrt{|m|}} \right) \right] \quad (9)$$

In the calculation, the parameters adopted in calculating eq. (4) and (5) are summarized in tabel (2), where the friction velocity and roughness length near the water surface and the bed are estimated from the observed velocity profiles. The calculated results were shown in Fig. 7 to Fig. 21, with thin solid curves names as R. It is shown that, nearly in all cases the Reid calculated results hold to a good approximation throughout the entire flow.

Theoretically, the shear stress within the flow is a linearly distributed over the depth, i.e.

$$\partial\tau/\partial Z = \frac{\tau_b}{Z_c + D} = \frac{-\tau_s}{Z_c} \quad (10)$$

and  $\tau_b = \rho_w U_{*b}^2$ ,  $\tau_s = \rho_w U_{*w}^2$ , ( $\rho_w$  is density of water), therefore the elevation  $Z_c$  where  $\tau = 0$  can be defined as

$$Z_c = D \frac{U_{*w}^2}{U_{*w}^2 + U_{*b}^2} \quad (11)$$

In this case, if we assume that the current profile can be approximated by fitting two logarithmic curves, one for the upper region, the wind induced current, and one for the lower region, the bottom part of the flow. These curves can be represented by

$$U(Z) - U_s = \frac{U_{*w}}{K} \ln \frac{Z}{Z_{ow}} \quad (Z \leq Z_c) \quad (12)$$

$$U(Z) = \frac{U_{*b}}{K} \ln \left( \frac{Z+D}{Z_{ob}} \right) \quad (Z \geq Z_c) \quad (13)$$

then, it is required that the value of the current estimated by eq. (12) be equal to that determined by eq. (13), when  $Z = Z_c$ , namely

$$U_s = \frac{U_{*b}}{K} \ln \left( \frac{Z_c+D}{Z_{ob}} \right) - \frac{U_{*w}}{K} \ln \frac{Z_c}{Z_{ow}} \quad (14)$$

The calculated distribution using eq. (12) and (13) are also shown in Fig. 7 to Fig. 21 indicated as L, the agreements are also acceptable in all cases.

The surface friction velocity which were estimated from the upper part of the observed velocity profiles are shown in Fig. 22, where  $U_{*w}$  is plotted against mean current velocity  $U_w$  with air velocity  $U_a$  as parameters. In all cases the  $U_{*w}$  values are close to those obtained from the air layer.

The bottom friction velocities  $U_{*b}$  were also plotted against mean current velocity  $U_w$  with air velocity  $U_a$  as parameters shown in Fig. 23.

It is well recognized that for turbulent flow in an open channel (no wind action). the shear stress  $\tau_b$  exerted by the fluid on the bottom is asserted to be of quadratic form as follows  $\tau_b = \lambda/8 \rho_w U_w^2$ , where  $\lambda$  is Darcy-Weisbach coefficient. Since  $\tau_b/\rho = U_{*b}^2$ , therefore,

$$U_{*b} = \sqrt{\frac{\lambda}{8}} U_w .$$

To estimate the  $\lambda$  value, the Blasius equation (ref. 11) is used in hydraulically smooth regime, i.e.

$$\lambda = 0.3164/Re^{1/4}$$

where  $Re$  is Reynold number defined as  $U_w.R/\nu_w$ , ( $R$  is wetted perimeter).

The relation  $U_{*b} = \sqrt{\frac{\lambda}{8}} U_w$  was also shown in Fig. 23 indicated as dash line. In all cases the friction velocity in the case of opposing wind action is larger than that in case of no wind action. As has been mentioned before, this graphically supports the findings that in the case of adverse wind, the velocity shear near the bed is larger than that of current only.

The  $m$  value which represents the ratio of bottom shear stress to surface shear stress is plotted as a function of the air velocity  $U_a$  with the mean current velocities as parameter in Fig. 24. It is shown that the magnitude of  $m$ , for a certain wind action, increases with increasing current velocity and the mean difference of  $m$  is greater in the case of lower wind velocities than of higher one. Further discuss on behaviour of the  $m$  value will be mentioned in paragraph VI.

V Water layer (following wind action)

In the case of the wind acts in the direction of the mean water flow, a rapid decrease of the velocity with depth will occur in the upper layers. This leads to the result that, for a given discharge, the velocity shear near the bottom is less than that which occurs in the absence of the wind.

Reid's (ref. 6) generalized formula for the velocity profile is summarized below.

The solutions for positive values  $m$  are separated into four cases, i.e.

$$\begin{aligned} \text{Case A} & \quad 0 \leq m \leq \gamma_0 / (1 + \gamma_0) \\ \text{case B} & \quad \gamma_0 / (1 + \gamma_0) \leq m \leq (1 + \gamma_1) / \gamma_1 \quad m \neq 1 \\ \text{case C} & \quad m = 1 \\ \text{case D} & \quad m \geq (1 + \gamma_1) / \gamma_1 \end{aligned}$$

The velocity distribution in different cases is represented as

case A:

$$\frac{U(Z)}{U_{*w}} = \frac{1}{K'} \left\{ 2 B_0 \left[ \tan^{-1} \frac{\gamma}{B_0} - \tan^{-1} \frac{\sqrt{m}}{B_0} \right] - B_1 \left[ \ln \frac{B_1 - \gamma}{B_1 + \gamma} - \ln \frac{B_1 - \sqrt{m}}{B_1 + \sqrt{m}} \right] \right\} \quad (16)$$

case B:

$$\frac{U(Z)}{U_{*w}} = \frac{1}{K'} \left\{ B_0 \ln \left[ \frac{(Y - B_0)(\sqrt{m} + B_0)}{(Y + B_0)(\sqrt{m} - B_0)} \right] - B_1 \ln \left[ \frac{(Y - B_1)(\sqrt{m} + B_1)}{(Y + B_1)(\sqrt{m} - B_1)} \right] \right\} \quad (17)$$

case C:

$$\frac{U(Z)}{U_{*w}} = \frac{1}{K'} \left[ \ln \frac{\gamma_0 + \zeta}{\zeta_0} - \ln \frac{1 + \gamma_1 + \zeta}{1 + \gamma_1} \right] \quad (18)$$

case D:

$$\frac{U(Z)}{U_{*w}} = \frac{1}{K'} \left\{ B_0 \ln \left[ \frac{(B_0 - Y)(B_0 + \sqrt{m})}{(B_0 + Y)(B_0 - \sqrt{m})} \right] - 2B_1 \left[ \tan^{-1} \frac{Y}{B_1} - \tan^{-1} \frac{\sqrt{m}}{B_0} \right] \right\} \quad (19)$$

And the mean currents are approximated below.

case A:

$$\frac{U_w}{U_{*w}} = \frac{2}{K'} \left\{ (1 - \sqrt{m}) - B_0 \left[ \tan^{-1} \frac{1}{B_0} - \tan^{-1} \frac{\sqrt{m}}{B_0} \right] \right\} \quad (20)$$

case B:

$$\frac{U_w}{U_{*w}} = \frac{2}{K'} \left\{ (1 - \sqrt{m}) + \frac{B_0}{2} \ln \left[ \frac{(\sqrt{m} + B_0)(1 - B_0)}{(\sqrt{m} - B_0)(1 + B_0)} \right] \right\} \quad (21)$$

case C:

$$\frac{U_w}{U_{*w}} = \frac{1}{K'} \ln \frac{1}{y_0} \quad (22)$$

case D:

$$\frac{U_w}{U_{*w}} = \frac{2}{K'} \left\{ (1 - \sqrt{m}) + \sqrt{m} \ln \frac{\sqrt{m}}{(1 + \sqrt{m})} + \frac{1}{2} \sqrt{m} \ln \frac{4}{y_0} \right\} \quad (23)$$

where  $Y$ ,  $B_0$ ,  $B_1$ ,  $K'$  etc. are defined by eq. (7).

By means of a similar procedure as mentioned in the case of adverse wind. the velocity distributions for the case of positive  $m$  are shown in Fig. (26 to 37). The parameters used in calculating Reid equation are

summarized in Table (3). The calculated results shown in Fig. (26 to 37) with solid curves are indicated with letter R. And the dash dot line curves represent the calculated results from 1/7 power law equation for current only.

As can be seen from the calculated results, the bottom friction velocities (Table 3) for following wind action are smaller than that of current only (Table 1) in all cases. And graphically from Fig. 26 to 37, it was shown that the current profiles are well approximated by Reid estimation noted as R which have relevance to equation 17 on case B only.

## VI The m character

In order to check the  $m$  value which represents the ratio of bottom shear stress to surface shear stress, it is plotted against the relative velocity  $U_r$  which is the ratio of mean current velocity  $U_w$  to surface friction velocity  $U_{*w}$  in Fig. 25 (the dash line represents the smooth curve of the data).

The state diagram appears to give a physically meaningful interpretation of measurements. In the case of opposing wind action the curve on the left hand side illustrates the general character of that  $m$  varies with relative velocity  $U_r$ . For instance, towards the horizontal axis for a given current flow ( $U_w$ ), the influence of the wind velocity shear is that the  $m$  value decreases with increasing the wind stress (i.e. to increase  $U_{*w}$ , decrease  $U_r$ ), which shows that the point of stress reversal is to be moved towards the bottom of the channel. Whereas for a given wind velocity shear (i.e. given  $U_{*w}$ ) the influence of the current flow is that the  $m$  value increases with increasing mean current velocity ( $U_w$ ), which shows that the point of stress reversal is to be moved towards the water surface. In the case of following wind action, the curve on the right hand side also illustrates the similar case of  $m$  behaviour.

The curve also shows that in the special case of mean current vanished, i.e.  $U_w = 0$ , it will meet the vertical  $m$  axis at a negative value. It can be explained that the situation above may exist if the shear stress exerted on the bottom by the fluid is opposite to that at the surface (i.e.  $m < 0$ ) and the flow in the lower layers of the channel being opposite to that at the surface. While in the special case of  $m = 0$ , i.e. there is no shear stress exerted on the bottom, the curve will meet the horizontal  $U_r$  axis at positive value and thus the entire curve remains to be a continuous transition from the case of negative  $m$  to that of positive  $m$ .

## VII Conclusion

The problem of turbulent flow structure of currents under the action of both opposing and following wind shear seems to have not yet been treated by many investigators. In Hiroichi Tsuruya's work (ref. 2), the turbulent structure of open-channel flow under the action of opposing wind shear was investigated, especially the changes induced in the mean velocity profiles, turbulent intensities and spectra and diffusion coefficient. However, the solution of the  $m$  value which is the ratio of bottom stress to surface stress was adopted as a constant without considering the influence of different current flow seems to be doubtful.

Systematic and simultaneous measurements have been made of the changes induced in the mean current velocity profiles in a wind-water tunnel. The result are found to support the findings that the current profile essentially follows the logarithmic law near the boundary layer, the air-water interface and the channel bed. And it is confirmed that the influence of the wind on the current profile in the case of a following wind is to give a smaller bottom friction than for current only, whereas for an opposing wind the bottom friction is larger than for current only. In the case of both opposing and following wind action, it is shown that the observed data are essentially well approximated by Reid's relations. Moreover, the velocity distribution of the flow with opposing wind can also be approximated by fitting two logarithmic curves. The  $m$  character, which represents the ratio of bottom stress to surface stress, may be illustrate as Fig. 25. Which shows the correlation between  $m$ , and  $U_r$  (ratio of mean current velocity  $U_w$  to surface friction velocity  $U_{*w}$ ). The curve illustrates that the  $m$  value increases with increasing the dimensionless mean velocity  $U_r$  and decreases with decreasing  $U_r$ .

Table 2, Parameters in calculating Reid equation ( $M < 0$ )

number	water				layer			
	$U_w$ cm/s	$U_a$ m/s	$U_s$ cm/s	$U_{*w}$ cm/s	$Z_{ow}$ cm	$U_{*b}$ cm/s	$Z_{ob}$ cm	-m
1		-3.7	-5.8	0.562	$2.91 \times 10^{-3}$	0.447	$2.19 \times 10^{-2}$	0.633
	4.75	-5.7	-11.5	0.929	$4.45 \times 10^{-3}$	0.571	$2.57 \times 10^{-2}$	0.378
		-8.0	-16.0	1.15	$4.45 \times 10^{-3}$	0.614	$1.89 \times 10^{-2}$	0.285
2		-3.7	3.0	0.616	$1.31 \times 10^{-2}$	0.70	$8.51 \times 10^{-3}$	1.291
	10.4	-5.7	-4.0	0.856	$3.65 \times 10^{-3}$	0.736	$5.53 \times 10^{-3}$	0.740
		-8.0	-5.0	1.277	$7.77 \times 10^{-3}$	0.965	$1.5 \times 10^{-2}$	0.571
3		-3.7	7.2	0.632	$6.55 \times 10^{-3}$	0.924	$6.66 \times 10^{-3}$	2.138
	14.1	-5.7	4.6	0.852	$2.66 \times 10^{-2}$	0.877	$4.86 \times 10^{-3}$	1.060
		-8.0	-2.6	1.182	$1.53 \times 10^{-2}$	0.965	$4.80 \times 10^{-3}$	0.667
4		-3.7	13.5	0.661	$3.34 \times 10^{-2}$	1.114	$6.29 \times 10^{-3}$	2.840
	18.0	-5.7	11.4	0.895	$6.57 \times 10^{-2}$	1.143	$4.91 \times 10^{-3}$	1.631
		-8.0	8.5	1.15	$8.9 \times 10^{-2}$	1.11	$3.15 \times 10^{-3}$	0.932
5		-3.7	15.4	0.709	$6.99 \times 10^{-3}$	1.259	$3.74 \times 10^{-3}$	3.153
	21.4	-5.7	10.0	0.90	$2.82 \times 10^{-3}$	1.401	$7.44 \times 10^{-3}$	2.420
		-8.0	6.5	1.128	$5.79 \times 10^{-3}$	1.316	$3.08 \times 10^{-3}$	1.361

air layer	no wind
$U_{*s}$ cm/s	$U_{*b}$ cm/s
0.551	
0.865	0.365
1.210	
0.606	
0.865	0.681
1.211	
0.673	
0.865	0.864
1.211	
0.673	
0.865	1.106
1.211	
0.673	
0.865	1.232
1.211	

Table 3. Parameters in calculating Reid equation ( $M > 0$ )

No	water layer							
	$U_w$ cm/s	$U_a$ m/s	$U_s$ cm/s	$U_{*w}$ cm/s	$Z_{ow}$ cm	$U_{*b}$ cm/s	$Z_{ob}$ cm	m
1	10.4	3.7	23.8	0.614	$2.929 \times 10^{-3}$	0.57	$1.52 \times 10^{-2}$	0.862
		5.7	28.6	0.856	$2.03 \times 10^{-3}$	0.364	$5.2 \times 10^{-4}$	0.181
		8.0	33.3	1.016	$1.12 \times 10^{-3}$	0.583	$3.79 \times 10^{-2}$	0.329
2	14.1	3.7	29.4	0.742	$6.86 \times 10^{-3}$	0.550	$6.05 \times 10^{-4}$	0.549
		5.7	35.7	0.905	$1.77 \times 10^{-3}$	0.823	$1.8 \times 10^{-2}$	0.827
		8.0	36.7	0.993	$9.97 \times 10^{-4}$	0.698	$1.34 \times 10^{-2}$	0.494
3	18.0	3.7	32.2	0.727	$1.55 \times 10^{-2}$	0.70	$3.7 \times 10^{-4}$	0.927
		5.7	38.5	0.929	$4.62 \times 10^{-3}$	0.87	$3.3 \times 10^{-3}$	0.877
		8.0	42.0	1.01	$1.44 \times 10^{-3}$	0.776	$1.87 \times 10^{-3}$	0.590
4	21.4	3.7	37.0	0.746	$1.19 \times 10^{-2}$	0.88	$5.33 \times 10^{-4}$	1.392
		5.7	41.7	0.864	$1.903 \times 10^{-3}$	0.783	$3.1 \times 10^{-4}$	0.821
		8.0	46.9	1.01	$1.28 \times 10^{-3}$	1.016	$2.68 \times 10^{-3}$	1.012

### Acknowledgements

I am expecting to depart Delft on March after two years of memorable association with the Laboratory of Fluid Mechanics in Delft University of Technology.

I should like the end of this note to be taken as a personal good-bye and expression of heartfelt thanks to all colleagues in the laboratory who have given me many helps and useful guidance. In particular, I am indebted to Prof.dr.ir. J.P.Th. Kalkwijk for his supervision of the work and review of several notes which I have completed during my staying in the laboratory.

## References

1. Wu, J. 1975. Wind-induced drift currents. *J. Fluid Mech.* 68, 49-70.
2. Hiroichi Tsuruya. 1985. Turbulent structure of currents under the action of wind shear. *J. Hydroscience and Hy. Eng.*, 3, no. 1, 23-43.
3. Douglas Baines, W. 1965. Wind driven water currents. *J. Hyd. Div. A.S.C.E.*, 91, 205-221.
4. Spillane, K.T. 1978. Wind-induced drift in contained bodies of water. *J. Phy. Oceanography* 8, 930-935.
5. Kranenburg, C. 1983. Wind-driven entrainment in a stably stratified fluid. Laboratory of Fluid Mechanics in Delft University of Technology, Report no. 83-3.
6. Reid, R.O. 1957. Modification of the quadratic bottom-stress law for turbulent channel flow in the presence of surface wind stress, tech. Memo, no. 93, Beach Erosion Board, Corps of Eng.
7. Baines, W.D. & Knapp, D.J. 1965. Wind driven water currents. *J. Hyd. Div. A.S.C.E.*, 91, 205-221.
8. Keulegan, G.H. 1951. Wind tides in small closed channels. *J. Res. Nat. Bur. Stand*, 46, 358-381.
9. Plate, E.J. 1970. Water surface velocity induced by wind shear. *J. Engng. Mech. Div. A.S.C.E.*, 96, 295-312.
10. Shemdin, O.H. 1972. Wind-generated current and phase speed of wind waves. *J. Phys. Oceanogr.*, 2, 411-419.
11. Chinghua hydraulic teaching group. 1980. *Hydraulics*. published by Science and Technology publishing company of China.
12. Hinze, J.O. 1975. *Turbulence*, 2nd ed. McGraw-Hill.

## Notation

$l$	mixing length
$m$	ratio of bottom stress to surface stress
$U(Z)$	longitudinal mean velocity at height $Z$
$U_w$	mean velocity of the section
$U_s$	surface velocity of the current
$U_{*a}$	friction velocity of air
$U_{*w}$	friction velocity of the stream at the free surface
$U_{*s}$	equivalent friction velocity $U_{*w}$ derived from air
$U_{*b}$	friction velocity at the channel bed
$x$	horizontal axis
$Z$	height above the mean water surface
$d$	water depth
$Z_{oa}$	roughness length of water surface for air layer
$Z_{ob}$	roughness length for the channel bed
$Z_{ow}$	roughness length for the free surface in water
$K$	Von Karman constant 0.4
$\zeta$	relative height measured from the bottom $D+Z/D$
$U_r$	ratio of mean velocity $U_w$ to surface friction velocity $U_{*w}$
$\nu_w$	kinematic viscosity of water
$\rho_a$	density of air
$\rho_w$	density of water
$\tau_b$	shear stress at the channel bed
$\tau_s$	shear stress at the free surface
$\tau$	shear stress within the flow

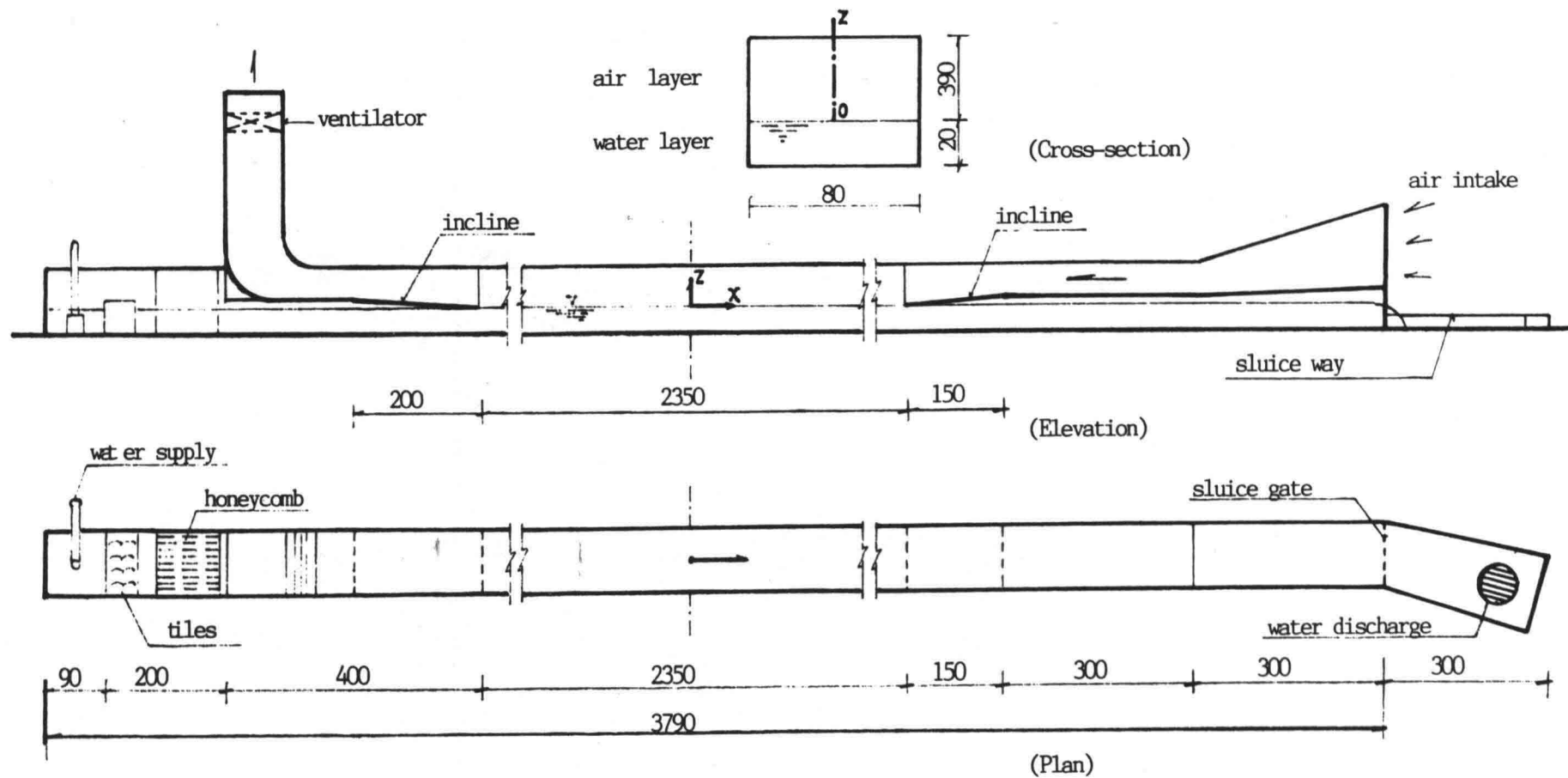


fig.1 Sketch of wind flume used in experiments on wind driven current

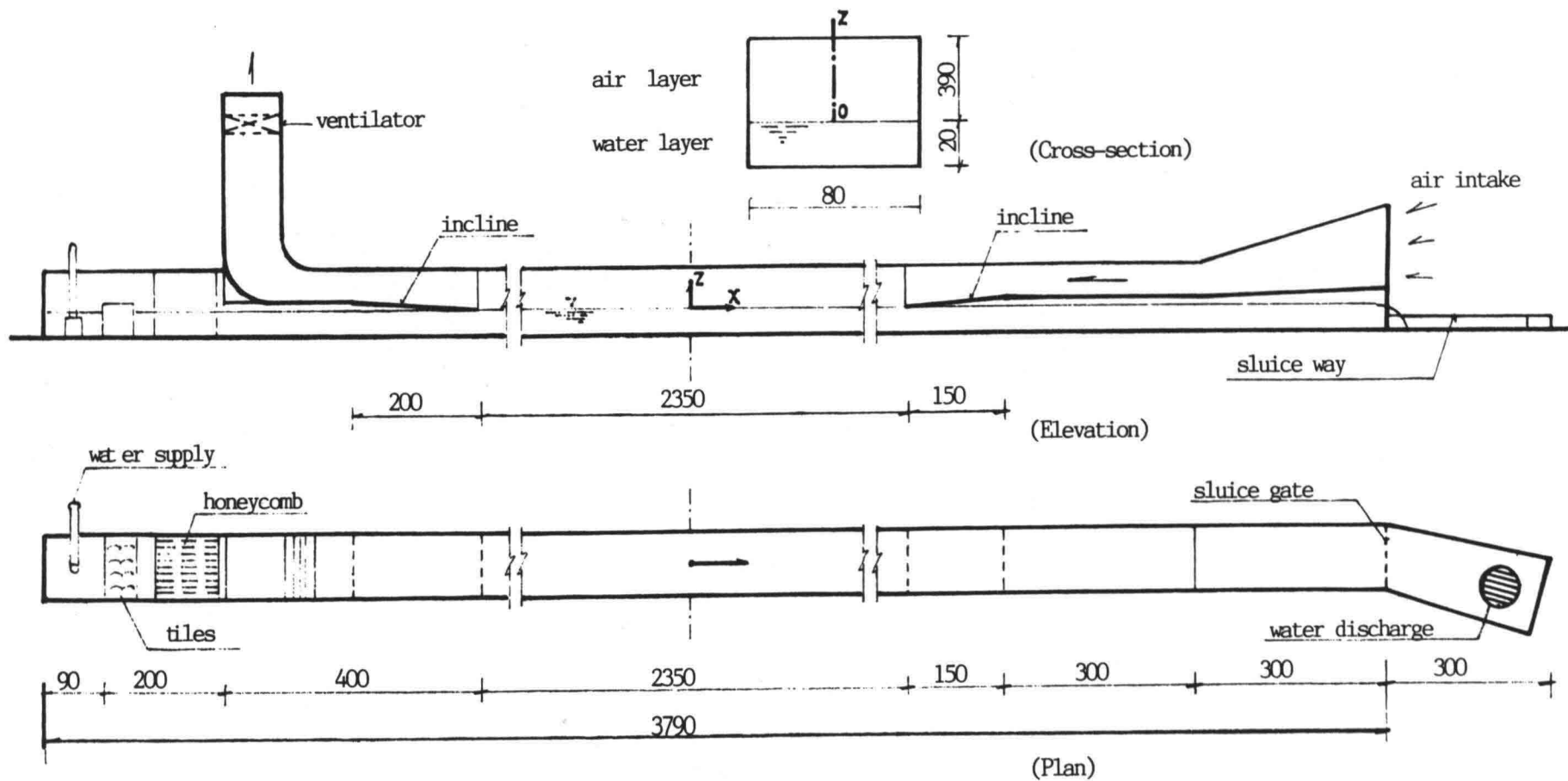
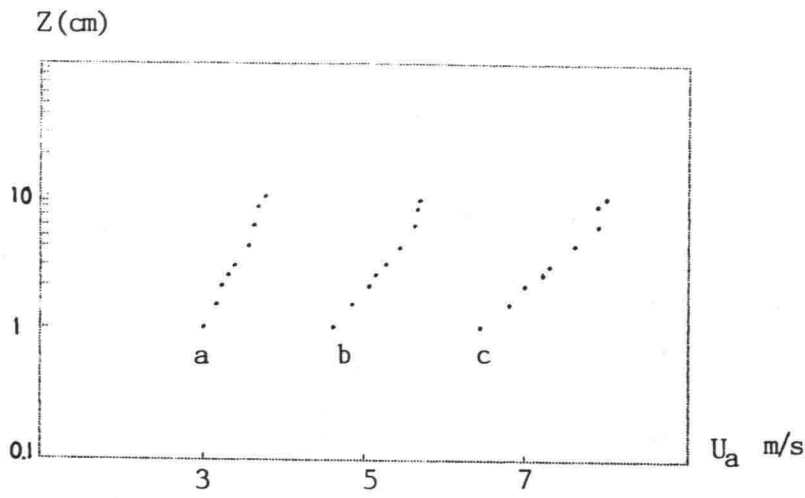
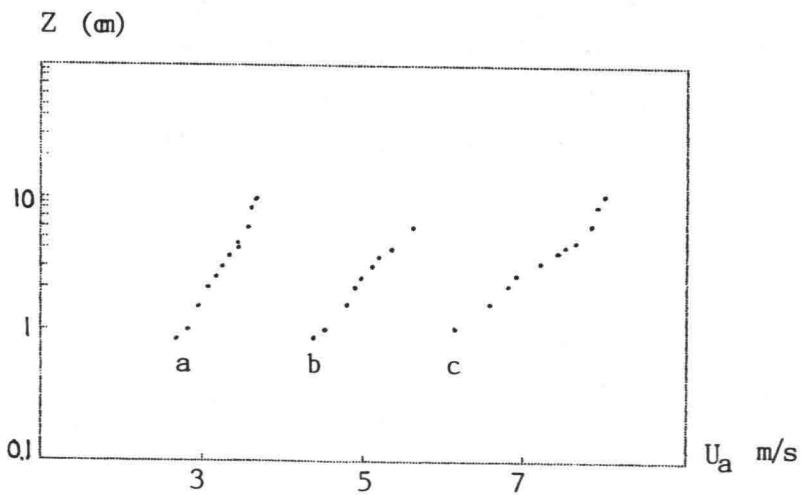


fig.1 Sketch of wind flume used in experiments on wind driven current



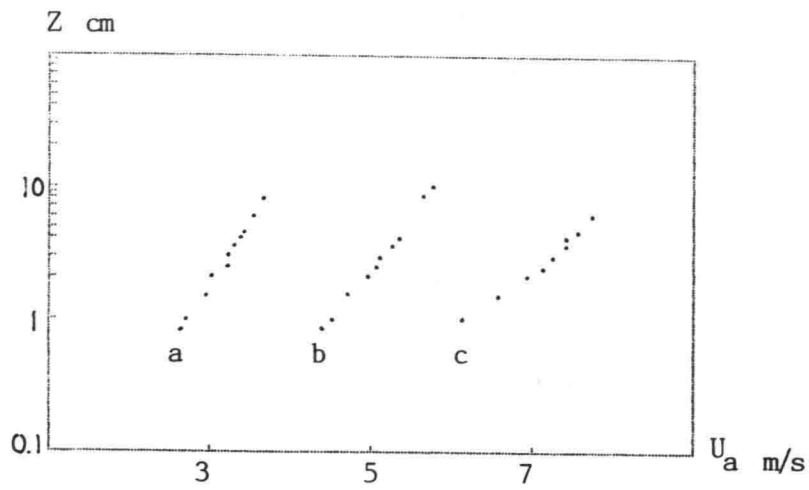
	$U_w$ cm/s	$U_a$ m/s
a)	4.75	3.7
b)	4.75	5.7
c)	4.75	8.0

fig. 2 Wind profiles



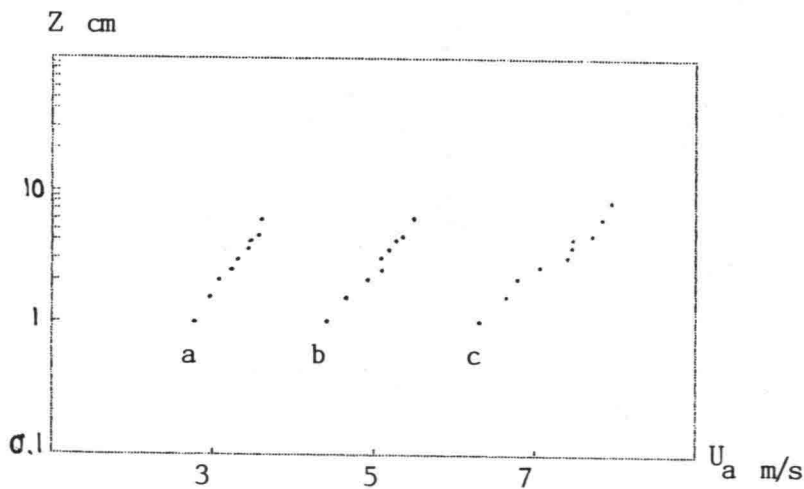
	$U_w$ cm/s	$U_a$ m/s
a)	10.4	3.7
b)	10.4	5.7
c)	10.4	8.0

fig. 3 Wind profiles



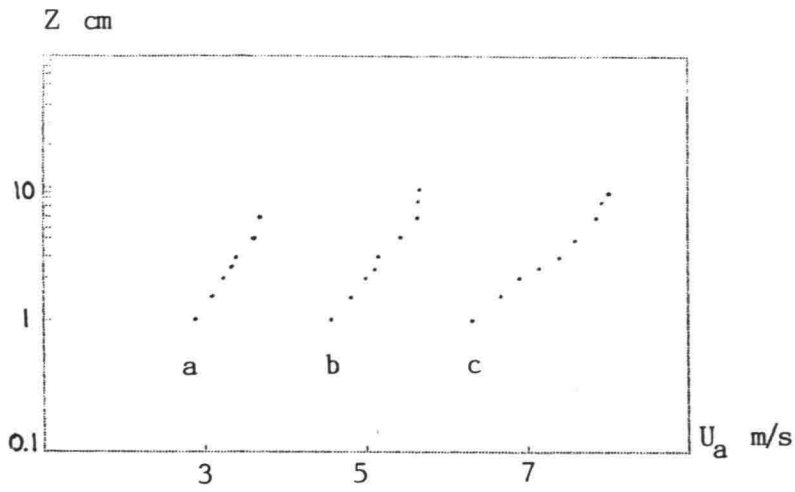
	$U_w$ cm/s	$U_a$
a)	14.7	3.7
b)	14.7	5.7
c)	14.7	8.0

fig. 4 Wind profiles



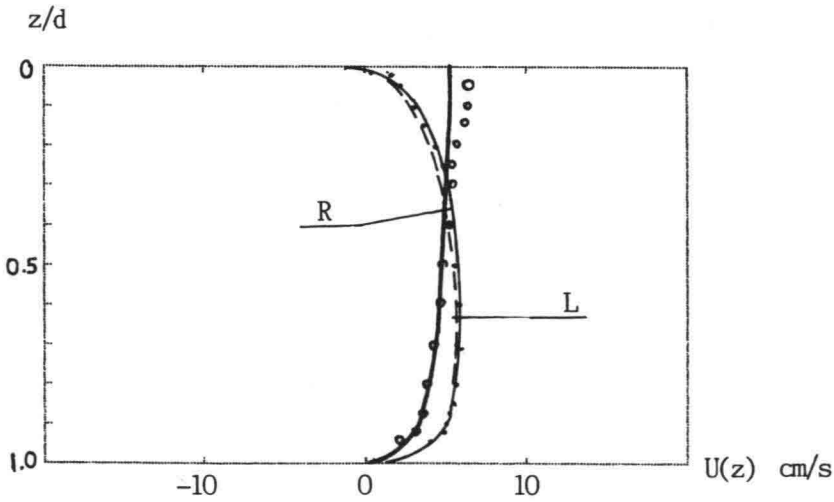
	$U_w$ cm/s	$U_a$ m/s
a)	18.0	3.7
b)	18.0	5.7
c)	18.0	8.0

fig. 5 Wind profiles



	$U_w$ cm/s	$U_a$ m/s
a)	21.4	3.7
b)	21.4	5.7
c)	21.4	8.0

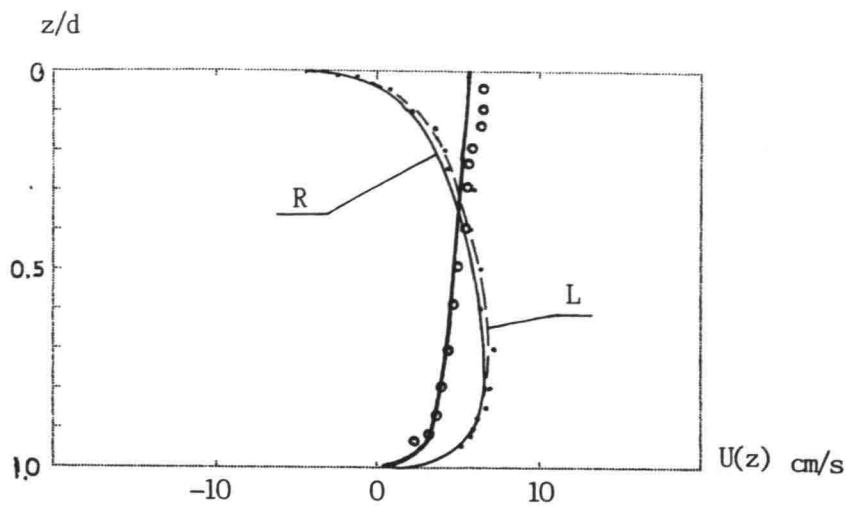
fig. 6 Wind profiles



$U_w$  4.75 cm/s  
 $U_a$  -3.7 m/s

- current only
- adverse wind

fig.7 Current profiles



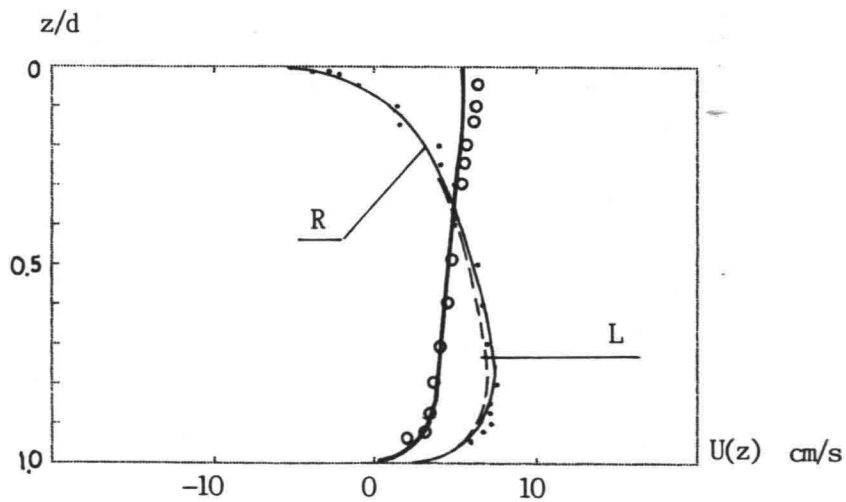
$U_w$  4.75 cm/s

$U_a$  -5.7 m/s

○ current only

● adverse wind

fig.8 Current profiles



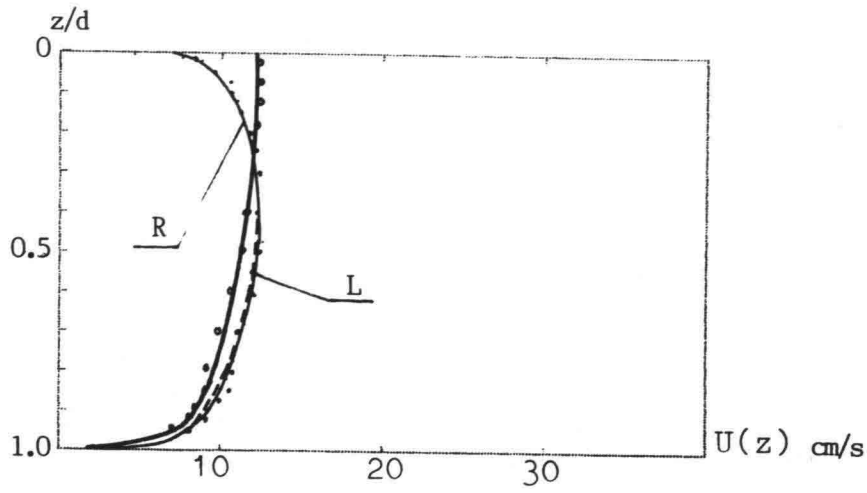
$U_w$  4.75 cm/s

$U_a$  -8.0 m/s

○ current only

● adverse wind

fig.9 Current profiles



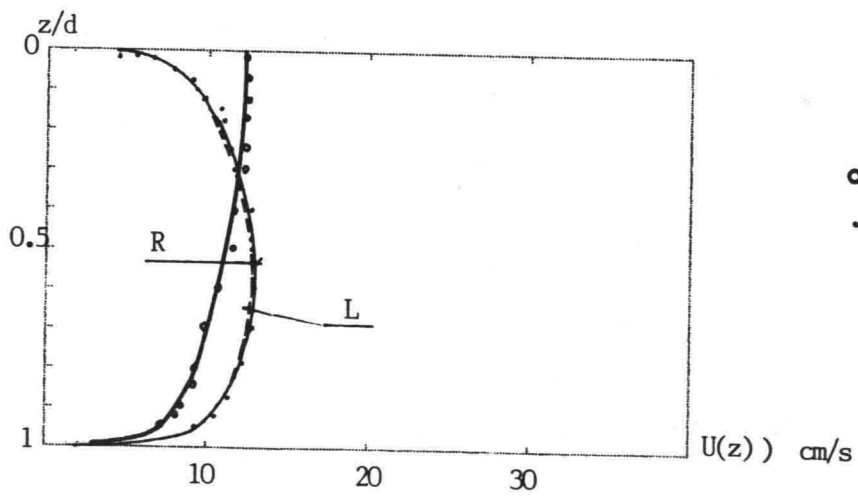
$U_w$  10.4 cm/s

$U_a$  -3.7 m/s

○ current only

• adverse wind

fig.10 Current profiles



$U_w$  10.4 cm/s

$U_a$  -5.7 m/s

○ current only

• adverse wind

fig. 11 current profiles

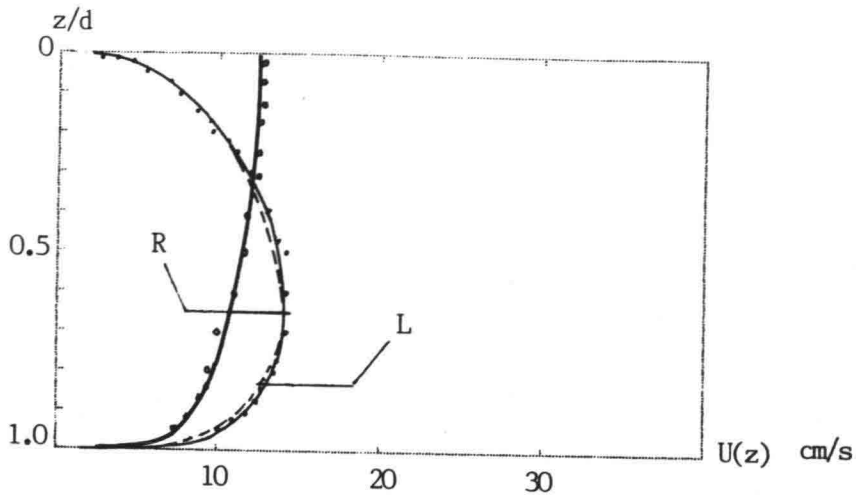


fig.12 Current profiles

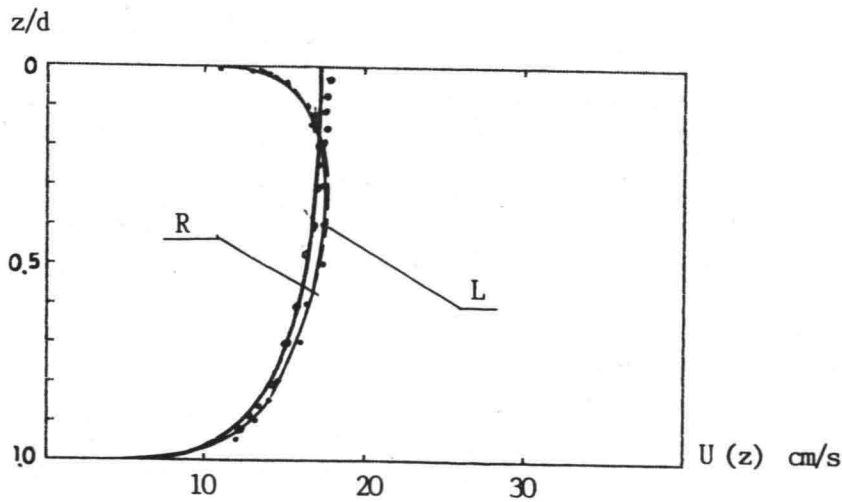


fig.13 Current profiles

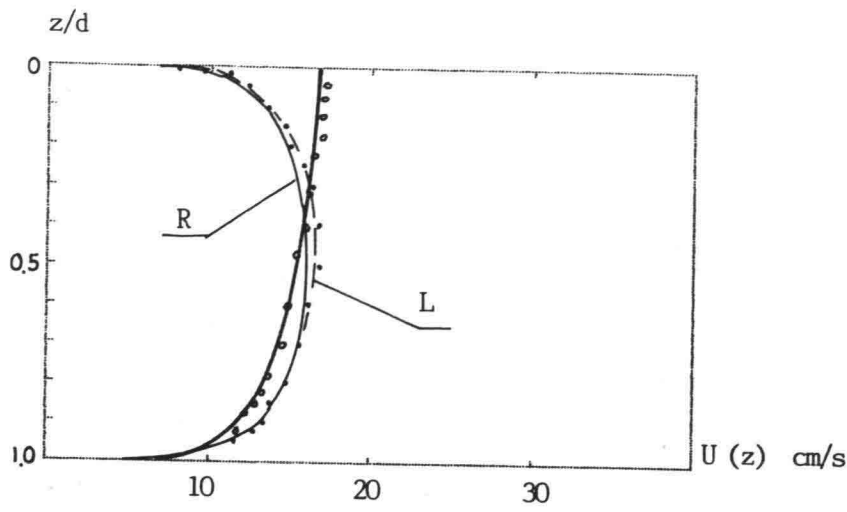


fig.14 Current profiles

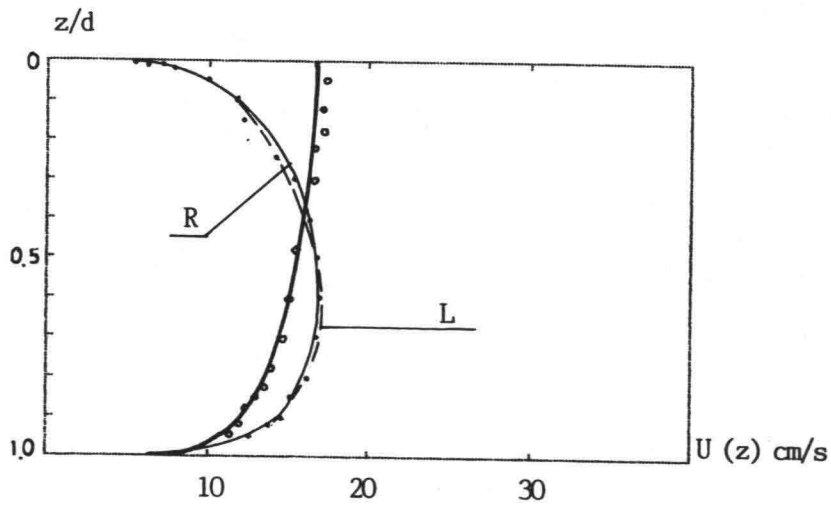


fig.15 Current profiles

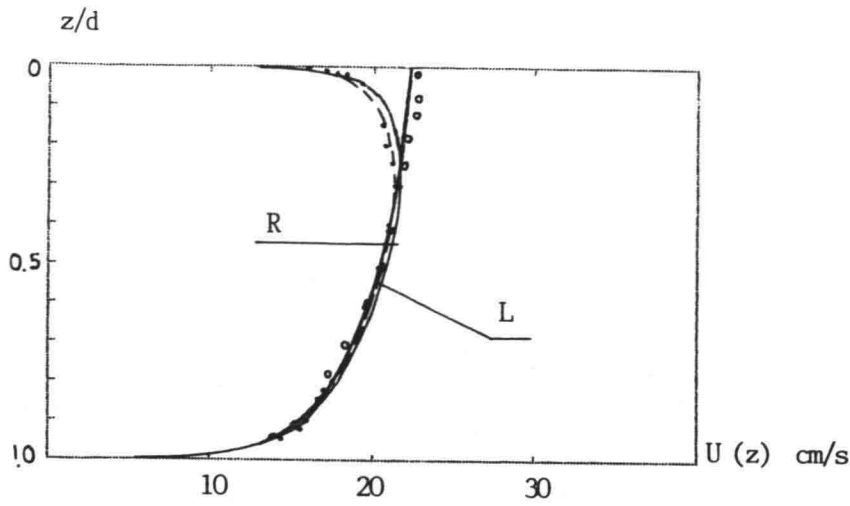


fig.16 Current profiles

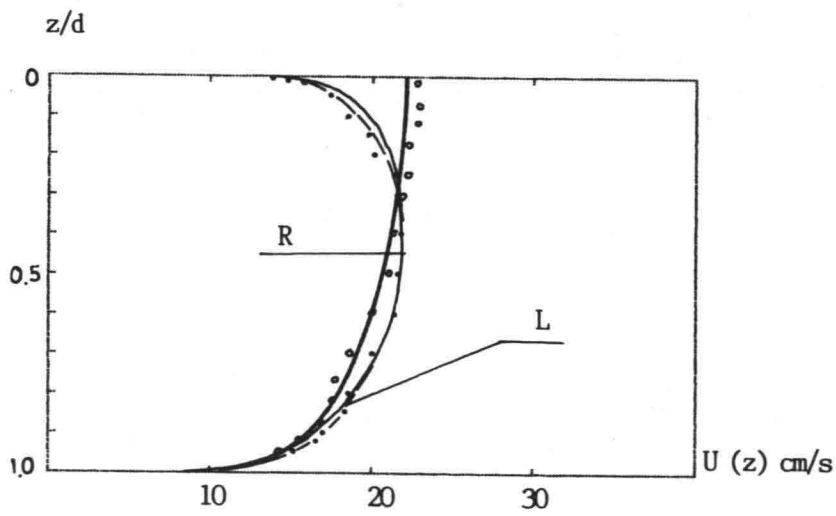


fig.17 Current profiles

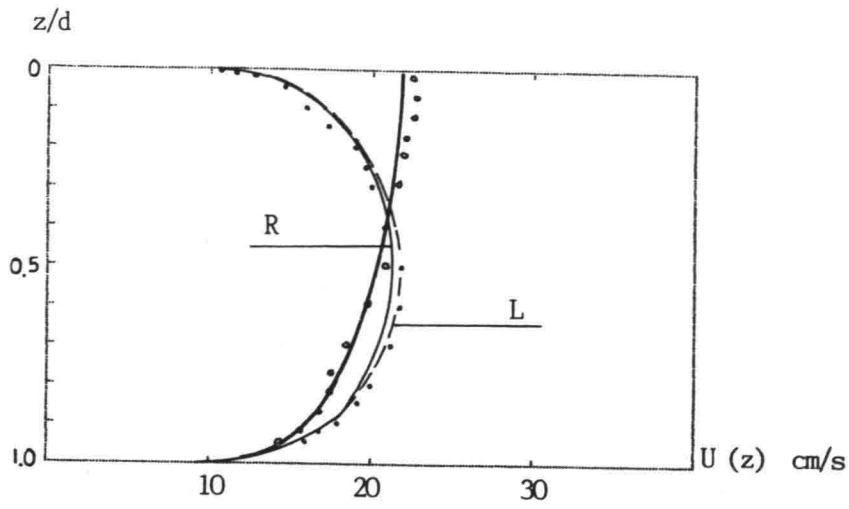


fig.18 Current profiles

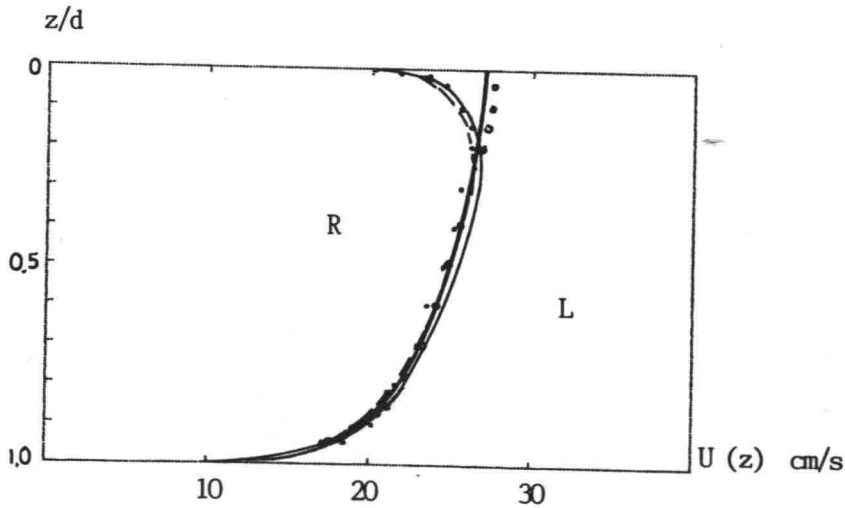
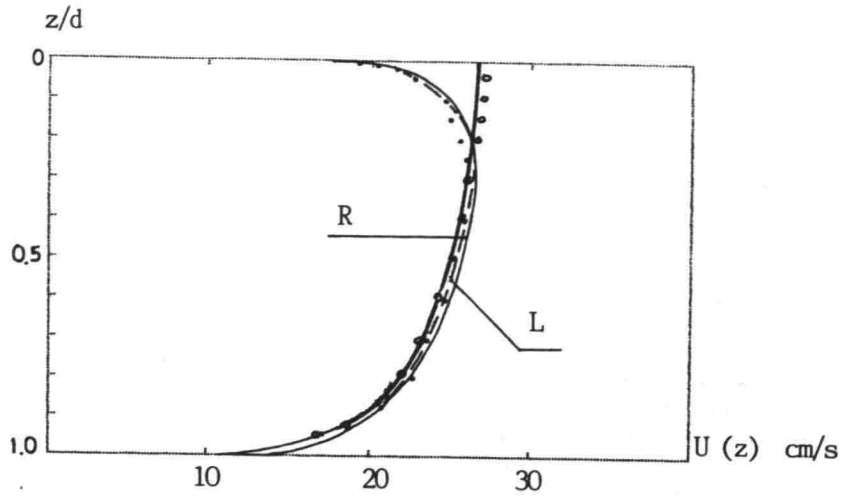
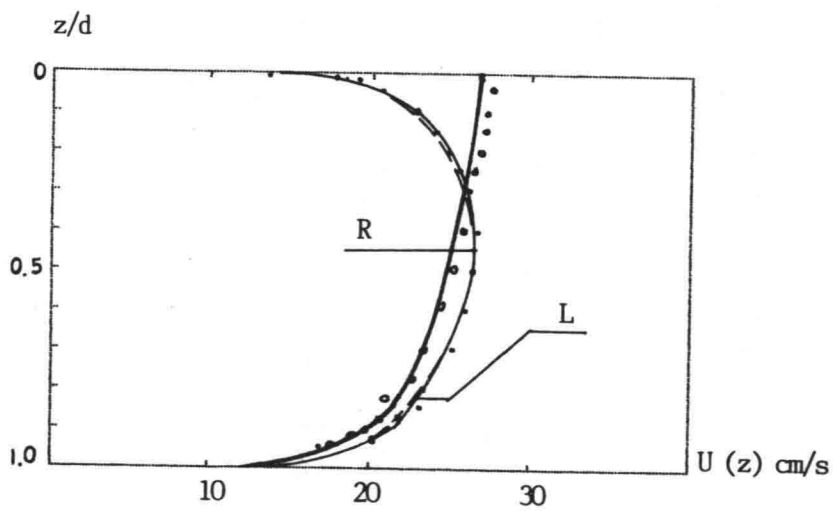


fig.19 Current profiles



$U_w$  21.4 cm/s  
 $U_a$  -5.7 m/s  
 ● current only  
 · adverse wind

fig.20 Current profiles



$U_w$  21.4 cm/s  
 $U_a$  -8.0 m/s  
 ● current only  
 · adverse wind

fig.21 Current profiles

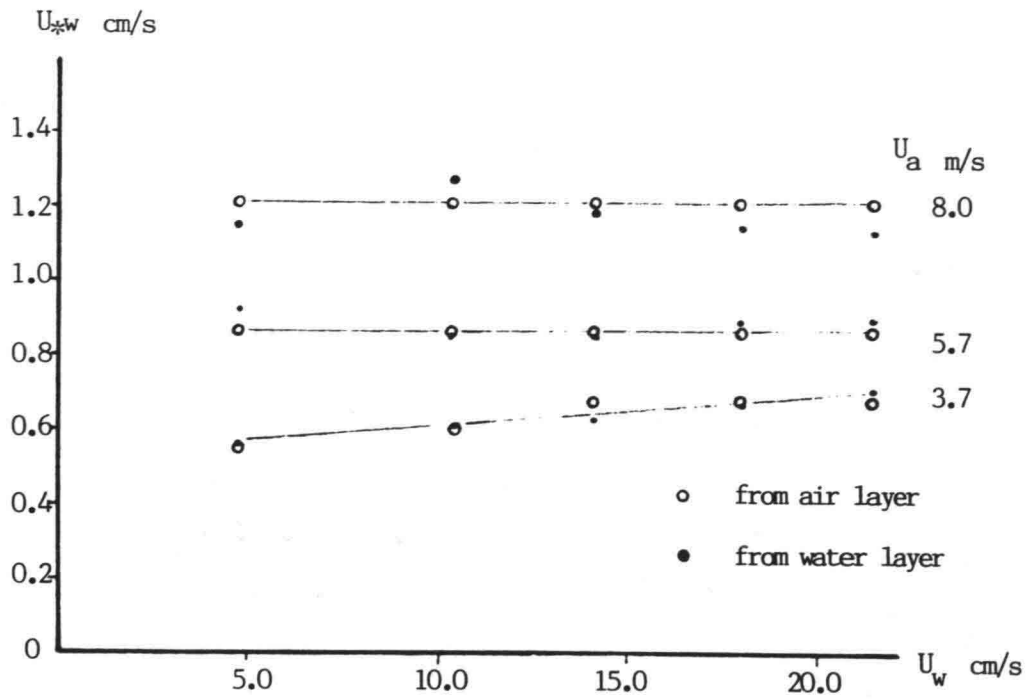


fig.22 Surface friction velocity

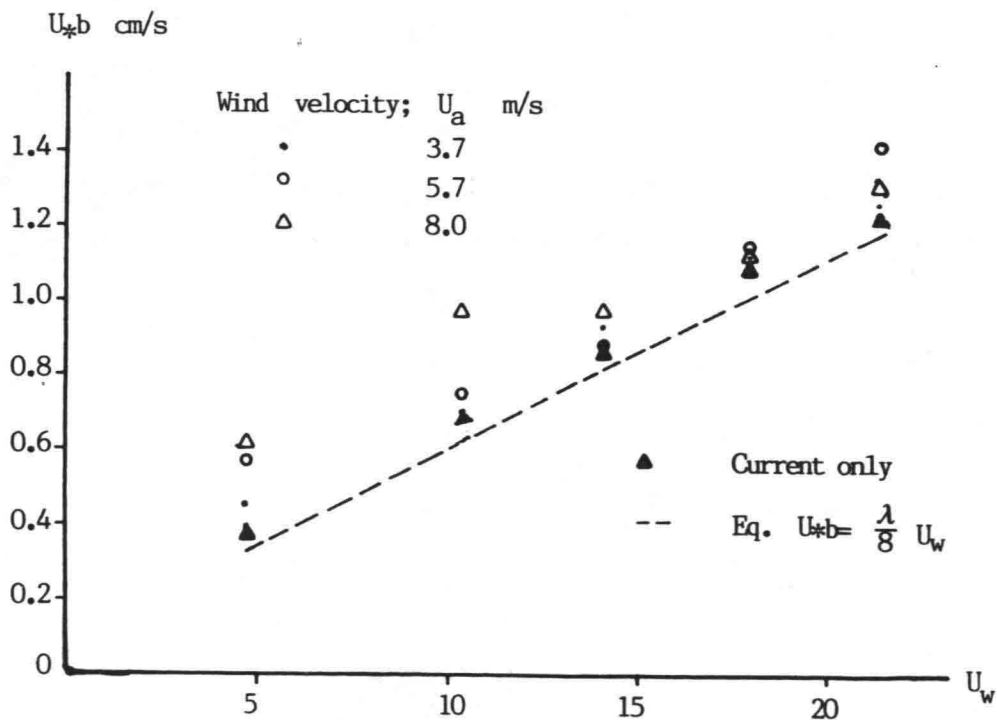


fig.23 Bed friction velocity

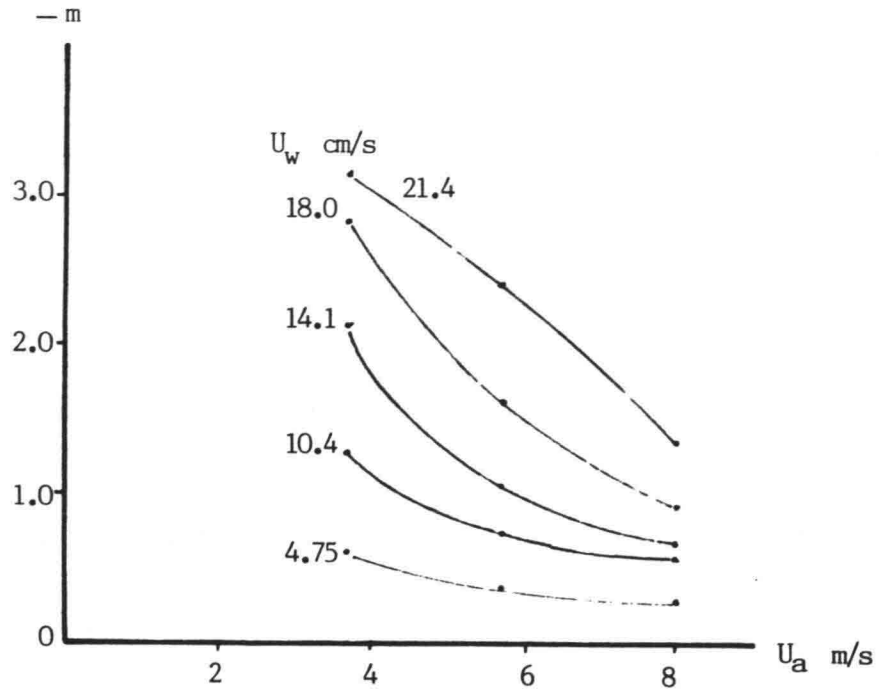


fig.24 Ratio of bottom stress to surface stress

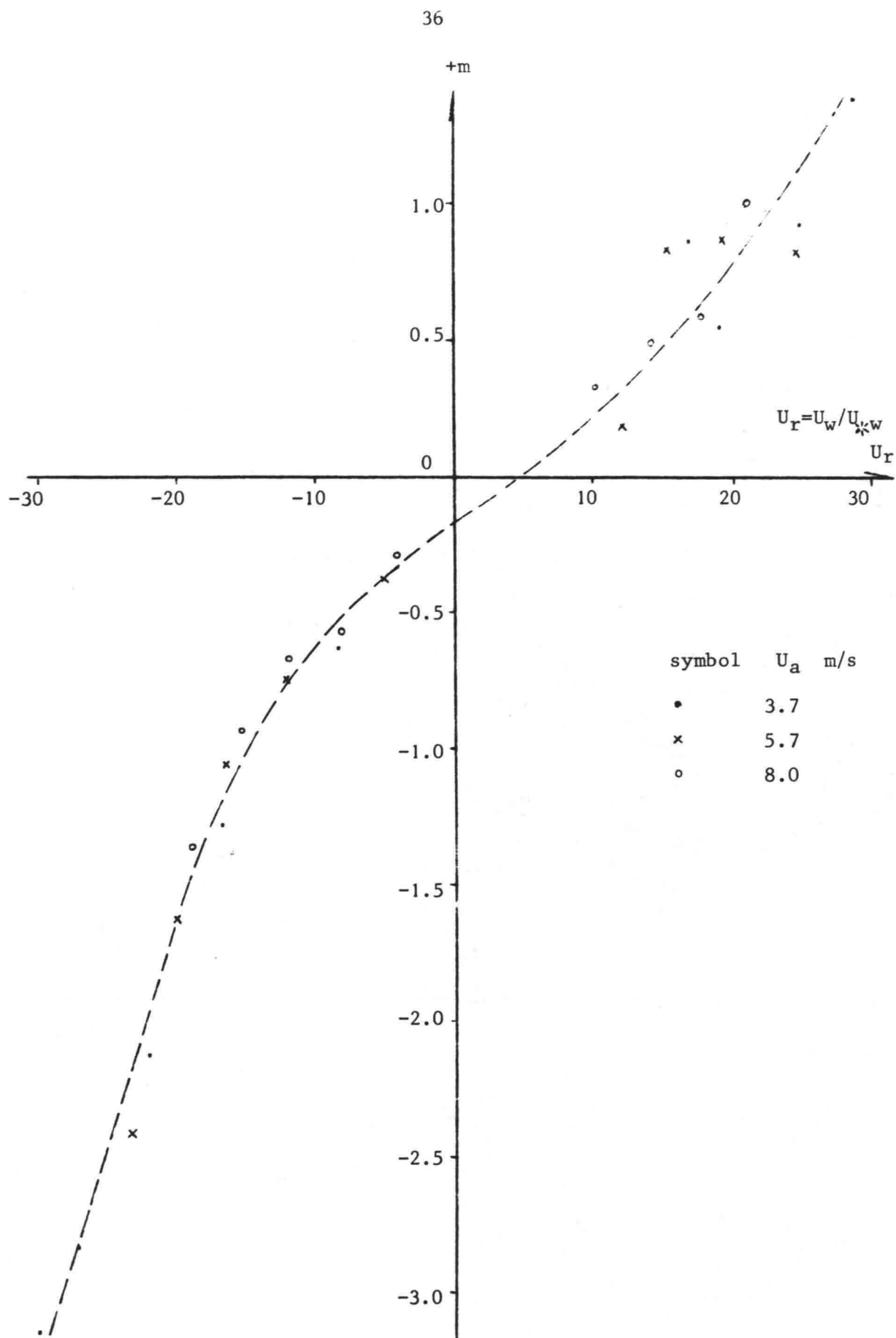


fig. 25 Plot of  $m$  versus  $U_r$

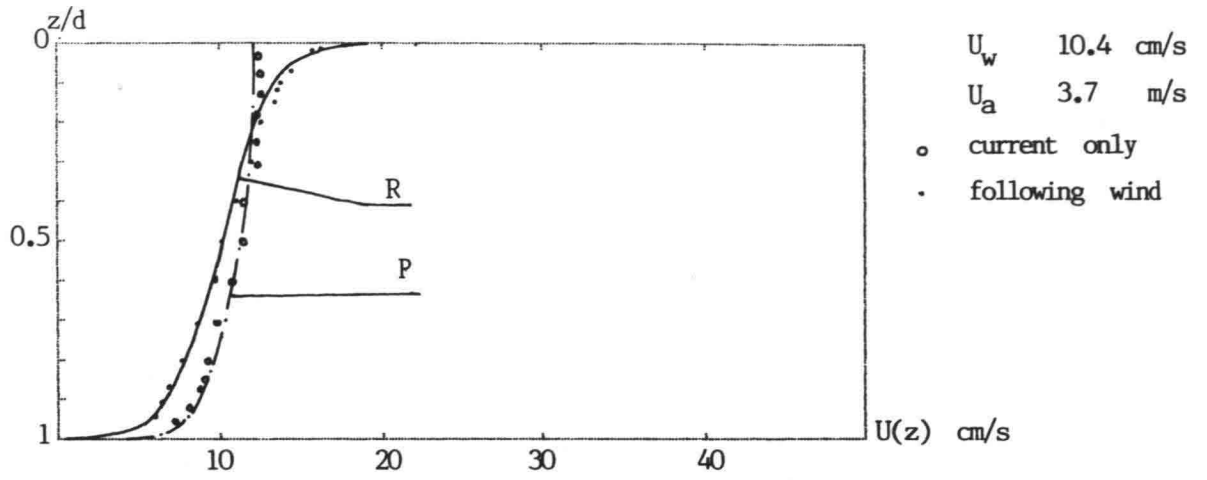


fig.26 Current profiles

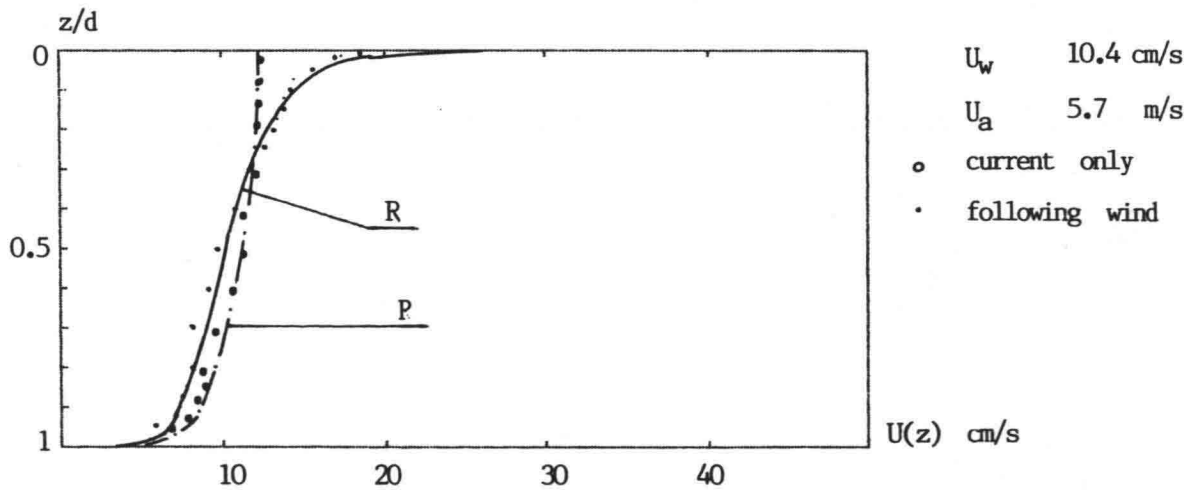


fig.27 Current profiles

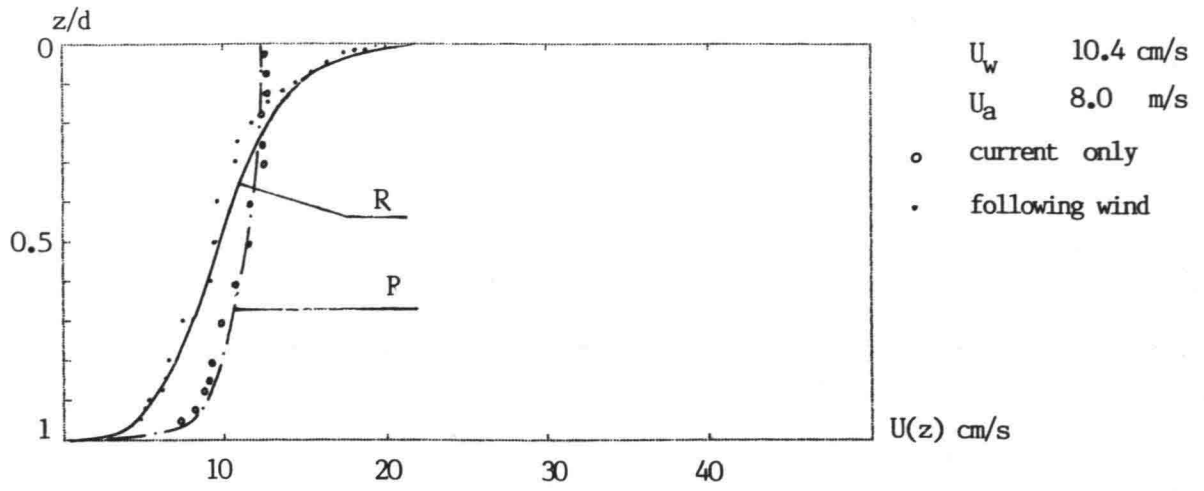


fig.28 Current profiles

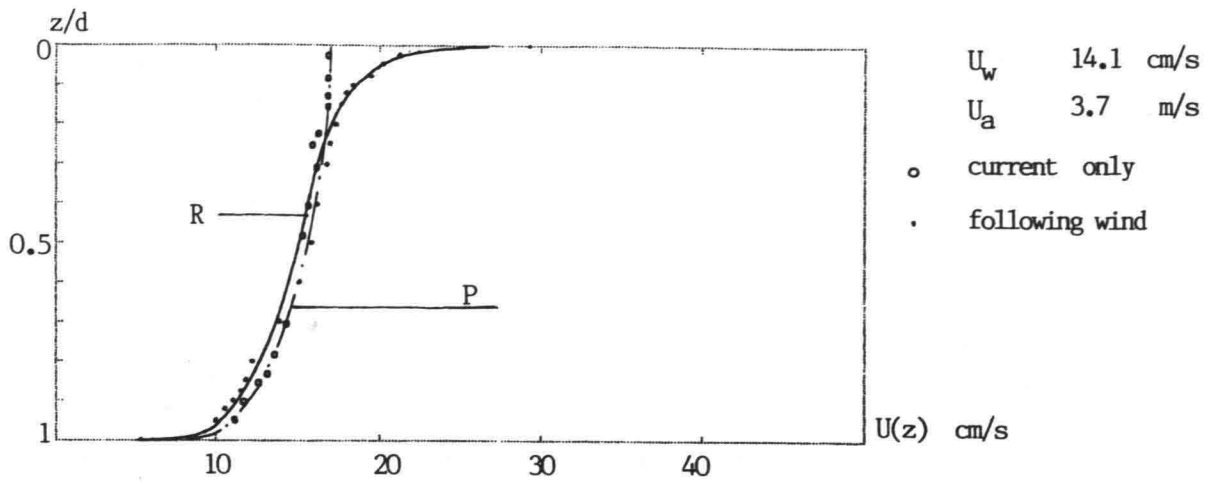


fig.29 Current profiles

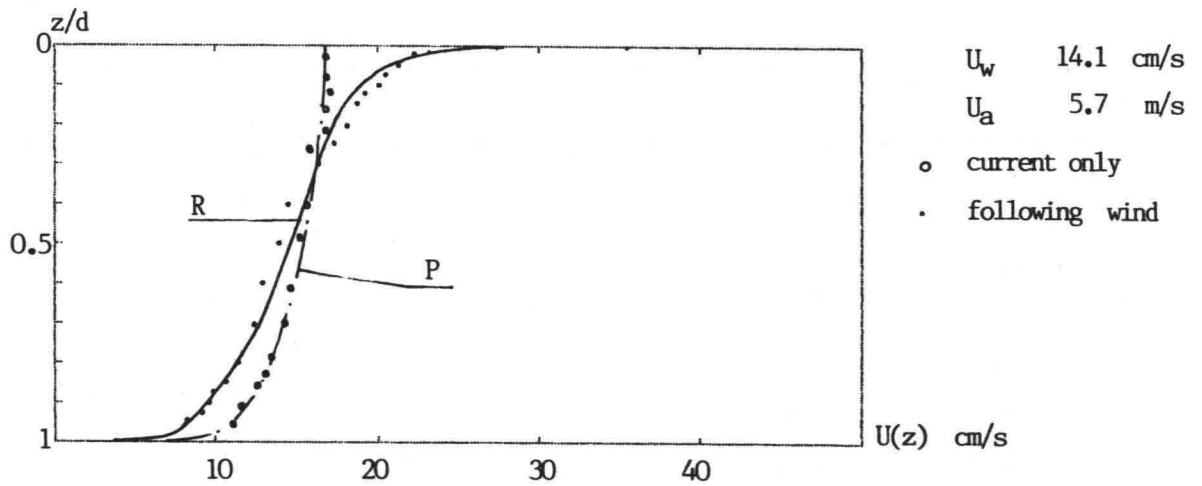


fig.30 Current profiles

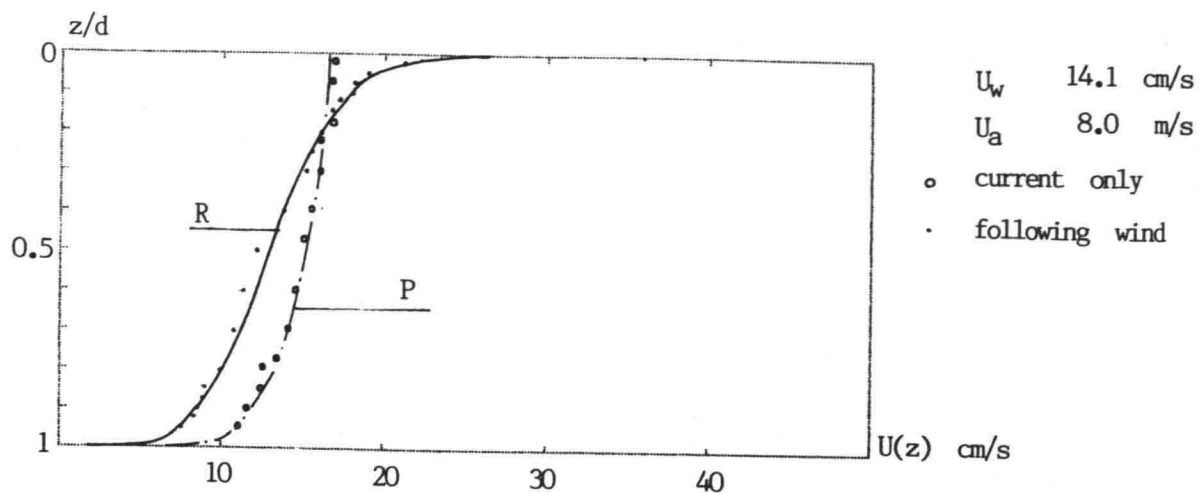


fig. 31 Current profiles

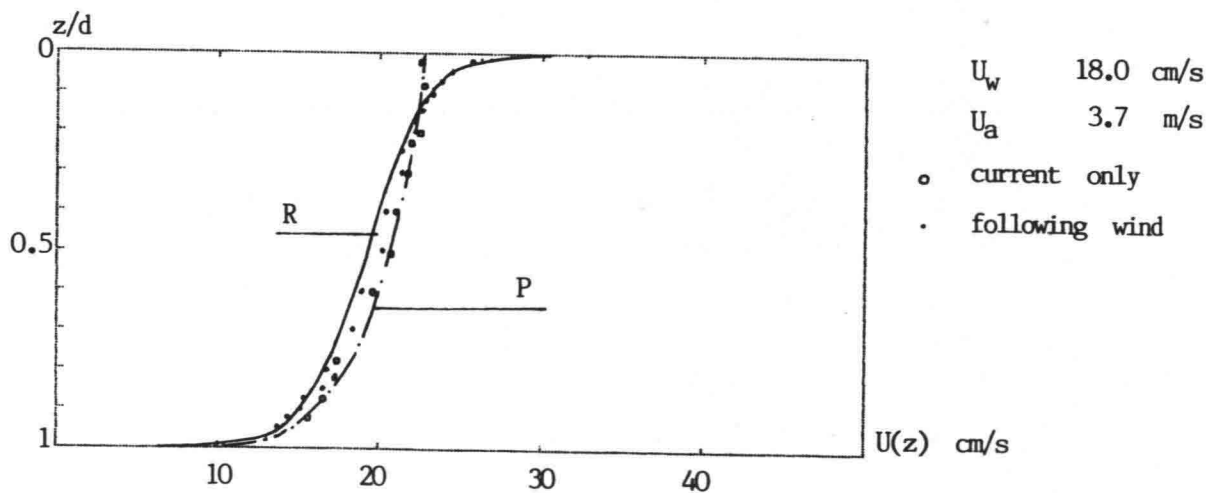


fig.32 Current profiles

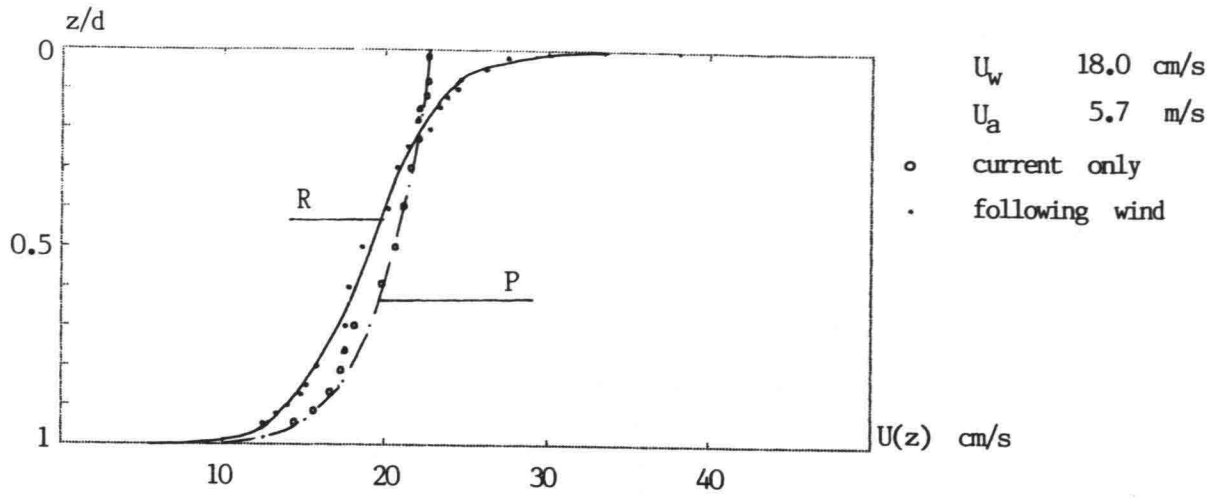


fig.33 Current profiles

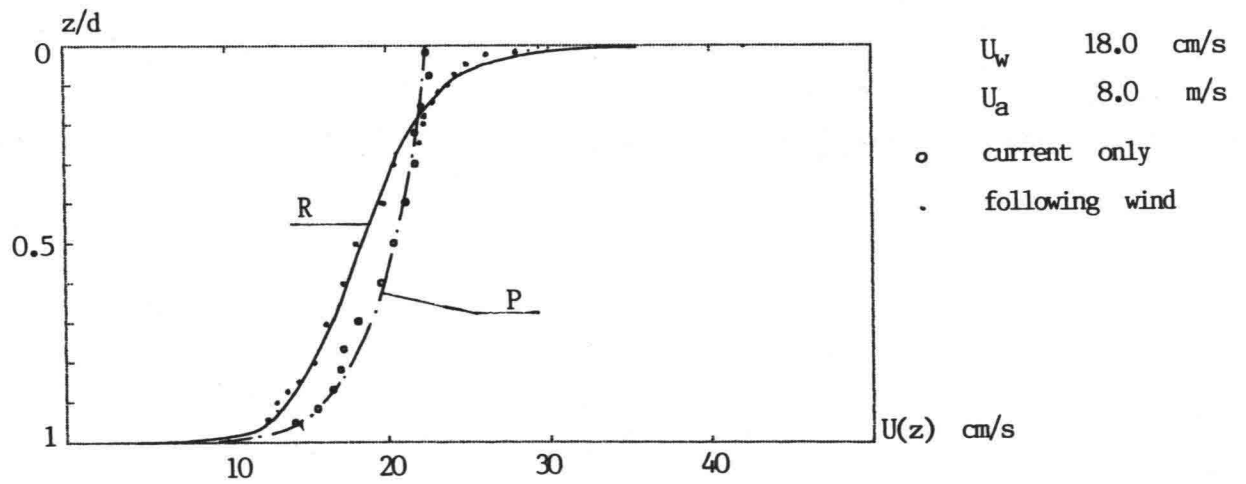


fig.34 Currnt profiles

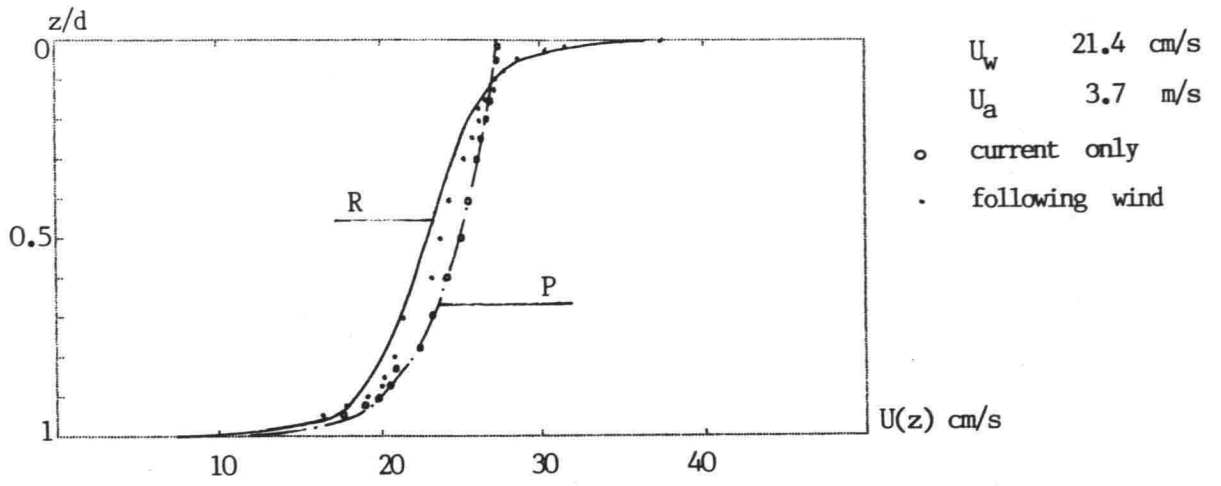


fig.35 Current profiles

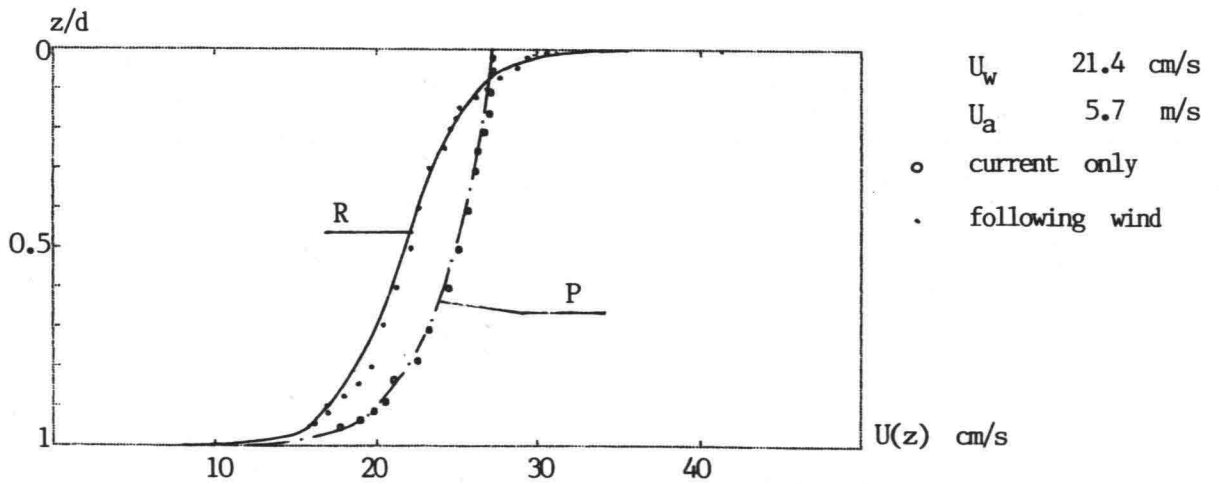


fig.36 Current Profiles

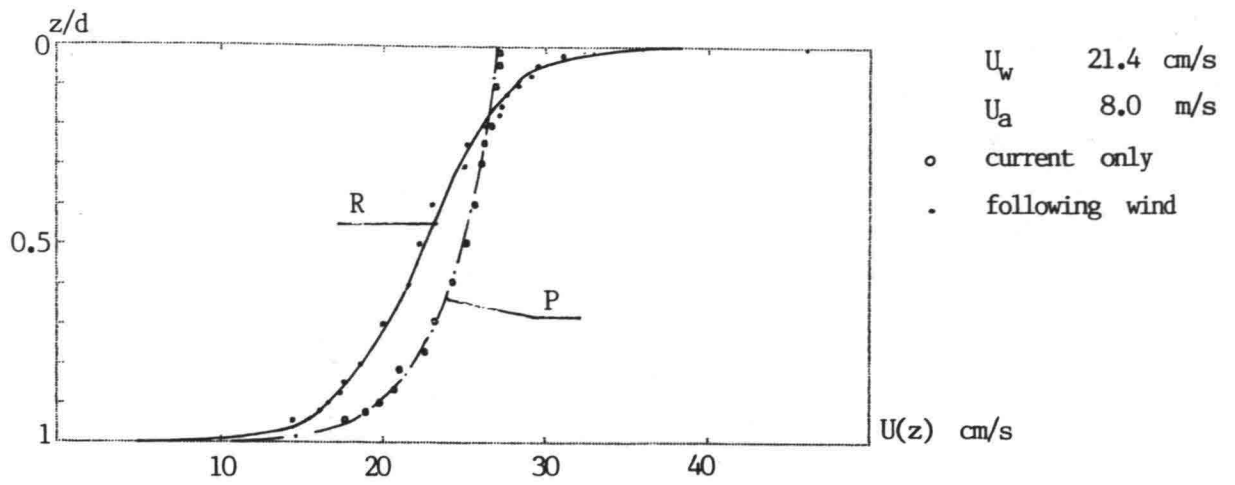


fig.37 Current profiles

